Approximate Analysis of Containment/Deflection Ring Responses to Engine Rotor Fragment Impact

Richard W.-H. Wu* and Emmett A. Witmer†
MIT, Cambridge, Mass.

The transient responses of containment and/or deflection rings to impact from an engine rotor-blade fragment are analyzed. Energy and momentum considerations are employed in an approximate analysis to predict the collision-induced velocities which are imparted to the fragment and to the affected ring segment. This collision analysis is combined with the spatial finite-element representation of the ring and a temporal finite-difference solution procedure to predict the resulting large transient elastic-plastic deformations of containment/deflection rings. Some comparisons with experimental data are given.

Introduction

SINCE the advent of the turbojet engine, there have been, from time to time, failures of turbine rotor blades, compressor rotor blades, and/or disks on engines of both military and civilian aircraft.[1-6] Fragments which are uncontained (that is, penetrate the engine and nacelle casing) might injure personnel occupying the aircraft and might cause additional damage to fuel lines and tanks, control systems, and other vital components. Although strenuous efforts have been and continue to be made to avoid blade/disk failures through improved materials, design, fabrication, and inspection, a not-insignificunt number of such failures persist. It is desirable, therefore, to provide protection a) for onboard personnel of aircraft in flight and b) for vital components.

Two distinct avenues for providing this protection are evident. First, the structure surrounding the failure-prone rotor region could be designed to contain (that is, prevent the escape of) the rotor-burst fragments completely. Second, the structure surrounding this rotor could be designed so as to prevent fragment penetration in, and to deflect fragments away from, certain critical regions or directions but to permit fragment escape readily in other harmless regions or directions. One or both of these schemes (see Fig. 1 schematic) could, in principle, be employed in a given design. In any event, this desired protection is sought for the least weight/cost penalty.

As pointed out in Ref. 1, NASA has been sponsoring a research program which is designed to meet the objective of providing the necessary protection to aircraft without imposing large weight penalties. Starting about 1964, the Naval Air Propulsion Test Center (NAPTC) under NASA sponsorship has constructed and employed a spin-chamber test facility wherein rotors of various sizes can be operated at high rpm, failed, and the interactions of the resulting fragments with various types of containment and/or deflection structures can be studied with high-speed photography (a very important capability and asset), in addition to post-mortem studies of the containment/deflection structure and the fragments. Many such tests involving single fragments or many complex fragments impinging upon containment structures of various types and materials have been conducted[2-6] and have substantially increased the body of knowledge of the attendant phenomena. For the past several years NASA has sponsored a research effort at the MIT Aeroelastic and Structures Research Laboratory (ASRL) to develop methods for predicting theoretically the interaction behavior between fragments and containment/deflection structures, as well as the transient deformations and responses of containment/deflection structures—the principal objective being to devise reliable prediction/design procedures and containment/deflection techniques. Important cross fertilization has occurred between the NAPTC experimental and the MIT-ASRL theoretical studies, with special supportive-diagnostic experiments and detailed measurements being designed jointly by NASA, NAPTC, and MIT personnel and conducted at the NAPTC. Subsequent analysis and theoretical-experimental correlation work has been increasing both the understanding of the phenomena involved and the ability to predict these interaction/structural-response phenomena quantitatively.

Selection of Analysis Method

Because of the multiple complexities involved in the very general case wherein, for example, the failure of one blade leads to impact against the engine casing, rebound, interaction with other blades and subsequent cascading rotor-failures and multiple-impact interactions of the various fragments with the casing and with each other, it is necessary to focus attention initially upon a much simpler situation in order to develop an understanding of these collision-interaction processes. Accordingly, rather than considering the general three-dimensional large deformations of actual engine casings under multiple rotor-fragment attack, the simpler problem of planar structural response of containment structures has been studied. That is, the containment structure is regarded simply as a structural ring lying in a plane; the ring may undergo large deformations but these deformations are confined essentially to that plane.

It has been demonstrated for planar structures such as beams and rings that accurate predictions of large deformation elastic-plastic transient responses of such struc-

Received July 20, 1972; revision received October 26, 1972. This research has been supported by the NASA Lewis Research Center under Grant NGR 22-009-339, with P. T. Chiarito serving as technical monitor and R. H. Kemp as technical advisor. The cooperation and helpful suggestions of Chiarito and Kemp are much appreciated. The authors are also indebted to G. J. Mangano and R. DeLucia of the Naval Air Propulsion Test Center, Philadelphia, Pa. for helpful suggestions and for supplying experimental data. Finally, we wish to express our appreciation to our colleagues J. W. Leech and R. P. Yeghiayan for their generous help and stimulating advice.

Index categories: Subsonic and Supersonic Airbreathing Propulsion; Aircraft Structural Design (Including Loads); Structural Dynamic Analysis.

*Research Engineer, Aeroelastic and Structures Research Laboratory, Department of Aeronautics and Astronautics.

†Professor of Aeronautics and Astronautics. Member AIAA.

tures with known mechanical properties can be obtained by the spatial finite-difference method[7] or by the spatial finite-element method[8,9] provided that one has accurate information on the distribution and time history of a) the externally-applied forces or b) the velocities externally-imparted to the structure. Therefore, the crucial information which needs to be determined (if the structural response of a containment ring is to be predicted reliably) concerns the magnitude, distribution, and time history of the loading or of the imparted velocities which the ring experiences because of fragment impact and interaction with the ring. Two means for supplying this information have been considered:

1) The TEJ concept[10,11] which utilizes measured experimental ring position-time data during the ring-fragment interaction process in order to deduce, by a backward solution of the equations of motion, the attendant external forces experienced by the ring. Such forces could then be applied tentatively in computer code response-prediction and materials-screening studies‡ for similar types of ring-fragment interaction problems involving various other materials, where guidance in the proper application of these forces or their modification could be furnished by dimensional-analysis[13] considerations and selected spot-check experiments. This approach suffers from the fact that experimental transient structural-deformation data must be available; the forcing function is not determined from basic material property, geometry, and initial impact information alone.

2) The second approach, however, utilizes basic material property, geometry, and initial impact information in an approximate analysis. The primary information predicted in this approach consists of either the collision-induced interaction forces or the collision-imparted velocities (or velocity increments); the associated and subsequent ring and fragment responses are also predicted.[8]

Approach 1 is explained in detail in Refs. 10, 11, and 14. The present paper deals with approach 2, and confines attention to problems involving only a single simple fragment; problems involving more complicated fragments are currently being studied.

Various levels of sophistication may be employed in approach 2. One could, for example, employ finite-difference methods wherein both the containment ring and the fragment are represented by a suitably fine three-dimensional spatial mesh; the conservation equations are solved in time for simple configurations by digital computer codes such as HEMP,[15] STRIDE,[16] and/or HELP,[17] which take into account elastic, plastic, strain hardening, and strain-rate behavior of the material. Such computations, while vital for certain types of problems, are very lengthy and expensive, and are not well suited for the type of engineering analysis/design purposes needed in the present problem; for complicated or multiple fragments, such calculations would be very complicated, lengthy, and expensive. A simpler, less complicated, engineering-analysis attack within this general framework is needed.

Two categories of such an engineering analysis may be identified and are termed: a) the collision-imparted velocity method (CIVM) and b) the collision-force method (CFM). The essence of each method follows:

a) Collision-Imparted Velocity Method (CIVM)—In this approach the local deformations of the fragment or of the ring at the collision interface do not enter explicitly, but the containment ring can deform in an elastic-plastic fashion by membrane and bending action as a result of having imparted to it a collision-induced velocity at the contact region via a) perfectly-elastic, b) perfectly-inelastic, or c) intermediate behavior. In fact, any type of material behavior may be accommodated readily. Since the collision analysis provides only collision imparted velocity information for the ring and the fragment (not the collision-induced interaction forces themselves), this procedure is called the collision-imparted velocity method.

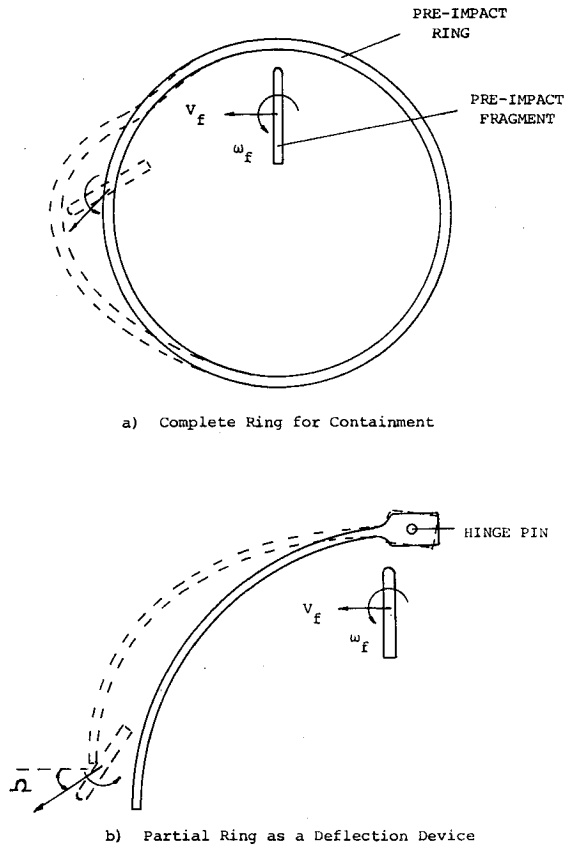

Fig. 1 Schematics of the fragment containment and fragment deflection problems.

b) Collision-Force Method (CFM)—In this method the primary information predicted in the collision analysis consists of the collision-induced interaction forces themselves; the associated and subsequent ring and fragment responses are also predicted.

In the present paper, only the collision-imparted velocity method (CIVM) is discussed; the status and developments pertinent to the collision force method (CFM) may be found in Refs. 8 and 18.

Accordingly, discussed in the following is an approximate collision analysis from which collision-imparted velocities to the impact-affected ring segment and to the fragment are obtained; these are then applied to a transient response code, wherein the structure is represented by finite elements, to predict the resulting transient structural response. This procedure is similar to that of Ref. 19 wherein the structure is represented by the spatial finite-difference method.

Following a description of the approximate collision analysis, the governing equations of motion for both the fragment and the containment ring structure are presented. Next, the solution procedure is described briefly. Then illustrative examples and comparisons with some experimental data are discussed. Finally, some aspects which are believed to be worthy of further study are noted.

Approximate Collision Analysis

Under consideration is an approximate method for predicting the immediate consequences of the impact of a single simple fragment against another physical body such as the ring shown in Fig. 2. The following simplifying as-

‡Studies of this type have been carried out.[12]

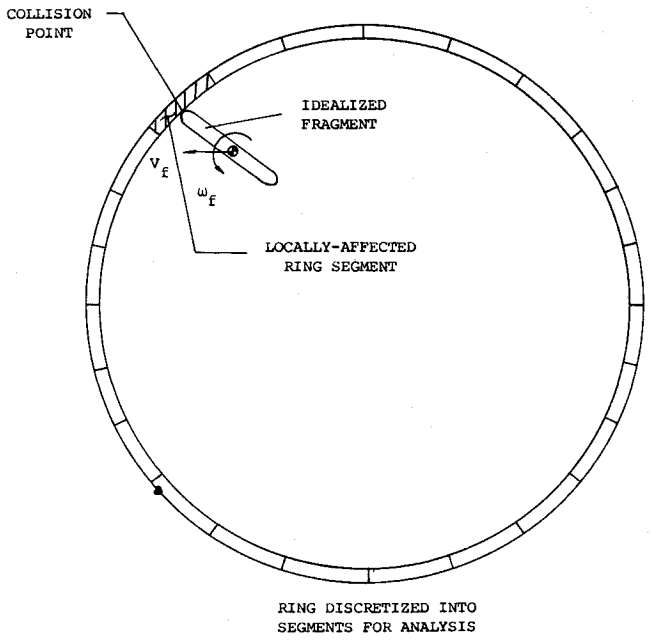

Fig. 2 Schematic of a containment ring subjected to single-fragment impact.

sumptions are invoked: 1) In an over-all sense, the fragment is treated as being rigid. It does not undergo bending or extensional deformations, but at the immediate contact region between the fragment and the struck object, the collision process is regarded as being instantaneous with a perfectly-elastic, a perfectly-inelastic, or an intermediate type of interaction. 2) The colliding surfaces of both the fragment and the target are perfectly smooth; hence, no forces and/or velocities (or momentum) are either transmitted or imparted in the tangential direction to the ring's surface at the impact point. 3) During the collision, the contact forces are the only ones considered to act on the fragment and (in an antiparallel fashion) on the ring. The change in the internal forces in the ring as a result of the current collision are approximated as being zero because the duration of the impact is so short as to preclude their effective development. 4) The collision process is instantaneous and involves only the fragment and the containment-ring segment which encompasses the ring-fragment collision point, as indicated schematically in Fig. 2. 5) To avoid unduly complicating the analysis and because of the smallness of the arc length of the target-ring element, the containment/deflection ring is treated as an assemblage of straight beams in the derivation of the impact equations (but by curved beams in the transient structural response analysis). Also, the mass of each ring element is considered to be concentrated at its two-end nodes as indicated in Fig. 3.

Since perfectly smooth surfaces for both the ring and the fragment are assumed to exist at the impact location, the instantaneous collision process results in an equal and opposite impulse, p_n, applied to the ring (beam) segment and to the fragment in the direction normal to the axis of the ring segment; accordingly, the tangential-component velocities are unaffected. Hence, only the normal-direction components of the velocities are considered in the impulse-momentum law and the kinetic energy conservation law used in order to characterize the instantaneous impact behavior of the system

Translational Impulse-Momentum Law

$$m_1[U_1' - U_1] + m_2[U_2' - U_2] = p_n \quad \text{(ring segment)} \quad (1)$$

$$m_f[U_f' - U_f] = -p_n \quad \text{(fragment)} \quad (2)$$

Rotational Impulse-Momentum Law

$$m_1[U_1' - U_1]\gamma S - m_2[U_2' - U_2]\delta S = -p_n(\alpha - \gamma)S \quad \text{(ring segment)} \quad (3)$$

$$I_f[\omega_f' - \omega_f] = p_n(l \sin\theta) \quad \text{(fragment)} \quad (4)$$

Kinetic Energy Conservation Law

$$1/2m_1(U_1')^2 + 1/2m_2(U_2')^2 + 1/2m_f(U_f')^2 + 1/2I_f(\omega_f')^2 + \text{(Energy Loss)} = 1/2m_1(U_1)^2 + 1/2m_2(U_2)^2 + 1/2m_f(U_f)^2 + 1/2I_f(\omega_f)^2 \quad (5)$$

where m_f is the mass of the fragment; I_f is the mass moment of inertia of the fragment about its center of gravity; m_1 and m_2 are point masses at nodes 1 and 2 of the ring segment which has a length s; U_1 and U_2 are the normal-direction velocity components at ring-element nodes 1 and 2 immediately before impact; U_f and ω_f are fragment c.g. normal-direction velocity component and angular velocity immediately before impact; and U_1', U_2', U_f', ω_f' are translational normal-direction velocities and the angular velocity immediately after impact.

Applying the concept of the coefficient of restitution, e, which is defined as the ratio of the relative speed of the ring and fragment at the impact point after impact to that before impact, Eq. (5) can be replaced by

$$[(\beta U_1' + \alpha U_2') - (U_f' - \omega_f' l \sin\theta)] = -e[(\beta U_1 + \alpha U_2) - (U_f - \omega_f l \sin\theta)] \quad (6)$$

Recall that $0 \leq e \leq 1$, where $e = 1$ represents a perfectly-elastic impact accompanying which no kinetic energy loss occurs. The condition $e = 0$ denotes a perfectly-inelastic impact for which the post-impact relative velocity of the colliding bodies is zero. For $e \neq 1$, there is a loss of kinetic energy; however, since the total energy must be conserved, the lost kinetic energy is simply converted to other forms such as thermal or heat energy, etc. which are ignored in the present mechanical analysis.

One can solve Eqs. (1–4) and Eq. (6) to obtain expressions for U_1', U_2', U_f', and ω_f', the after-impact quantities

$$U_1' = U_1 - m_2\beta(1 + e)U_R/K \quad (7)$$

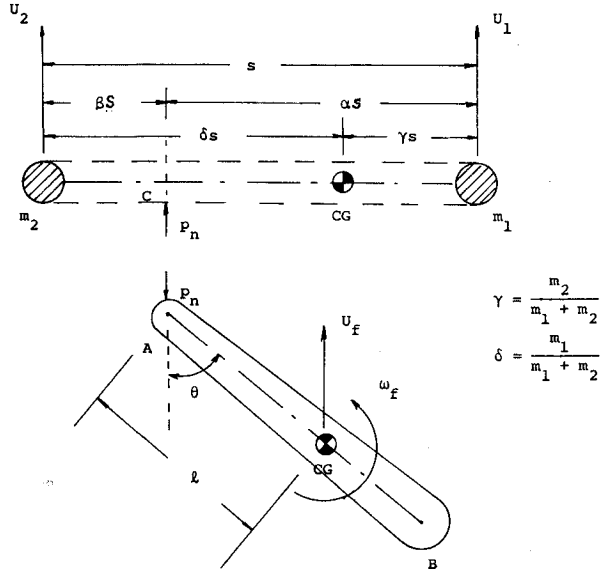

Fig. 3 Schematic of the collision model for the fragment against a ring segment.

$$U_2' = U_2 - m_1\alpha(1 + e)U_R/K \tag{8}$$

$$U_f' = U_f + (m_1m_2/m_f)(1 + e)U_R/K \tag{9}$$

$$\omega_f' = \omega_f - (m_1m_2/I_f)(l \sin\theta)(1 + e)U_R/K \tag{10}$$

where

$$K = (m_1m_2/m_f) + m_1\alpha^2 + m_2\beta^2 + (m_1m_2/I_f)(l \sin\theta)^2$$

and

$$U_R = (\beta U_1 + \alpha U_2) - (U_f - \omega_f l \sin\theta)$$

$$\equiv U_C - U_A = \text{relative velocity of the impact points } C \text{ and } A.$$

Governing Equations

Ring-Structure Motion

The assumed displacement form of the spatial finite-element representation is utilized in conjunction with the Principle of Virtual Work and D'Alembert's Principle to obtain the equations of motion for a ring structure which is permitted to undergo large-deflection elastic-plastic transient deformation[8,9,20]

$$[M^*]\{\ddot{q}^*\} + \{P^*\} + [H^*]\{q^*\} = \{F^*\} \tag{11}$$

where $\{q^*\}$, $\{\ddot{q}^*\}$ represent the generalized displacements and generalized accelerations, respectively, for the complete assembled discretized ring structure (the asterisk as in Ref. 8 means that these quantities are defined with respect to a global coordinate system); $[M^*]$ is the mass matrix for the complete assembled discretized structure; $\{F^*\}$ is the assembled vector of externally-applied loading; $\{P^*\}$ is an assembled internal force matrix which replaces the conventional stiffness[8,21] terms $[K^*]\{q^*\}$ for small displacements but also includes some plastic behavior contributions; and $[H^*]\{q^*\}$ represents generalized loads arising from both large deflections and also plastic behavior. As explained in Ref. 8, the quantities $\{P^*\}$ and $[H^*]$ are found by the numerical evaluation by Gaussian quadrature of pertinent volume integrals of each ring finite element, and then assembling this information for the entire structure in global coordinate form.

Note that Eq. (11) represents the unconventional form of the equations of motion. The conventional form of these equations as defined, for example, in Refs. 8 and 21 could also be used, if desired.

The timewise solution of Eq. (11) may be accomplished by employing an appropriate timewise finite-difference scheme such as the central difference method, for example. Equation (11) at time instant j may be written in the form

$$[M^*]\{\ddot{q}^*\}_j = (\{F^*\} - \{P^*\} - [H^*]\{q^*\})_j \tag{12}$$

Let it be assumed that all quantities are known at any given time instant t_j. Then one may determine the generalized displacement solution at time t_{j+1} (i.e., $\{q^*\}_{j+1}$) by the following procedure. First, one employs the timewise central-difference expression for the acceleration $\{\ddot{q}^*\}_j$

$$\{\ddot{q}^*\}_j = (\{q^*\}_{j+1} - 2\{q^*\}_j + \{q^*\}_{j-1})/(\Delta t)^2 \tag{12a}$$

It follows that one can solve for $\{q^*\}_{j+1}$ since $\{\ddot{q}^*\}_j$ is already known from Eq. (12) and all other quantities in Eq. (12a) are known. However, a fragment-ring collision may occur between time instants t_j and t_{j+1}; this would require a correction to the $\{q^*\}_{j+1}$ found from Eq. (12a). Thus, one uses and rewrites Eq. (12a) to form a trial value (overbar):

$$\{\Delta\bar{q}^*\}_{j+1} = \{\Delta q^*\}_j + (\Delta t)^2\{\ddot{q}^*\}_j \tag{12b}$$

where

$$\{\Delta q^*\}_j = \{q^*\}_j - \{q^*\}_{j-1}$$

$$\{\Delta\bar{q}^*\}_{j+1} = \{\bar{q}^*\}_{j+1} - \{q^*\}_j = \text{trial increment}$$

$$\{q^*\}_j = \{q^*\}_0 + \{\Delta q^*\}_1 + \{\Delta q^*\}_2 + \cdots + \{\Delta q^*\}_j$$

Δt = time increment step§

Note that $t_j = j(\Delta t)$ where $j = 0, 1, 2, \ldots$, and $\{\Delta q^*\}_0 \equiv 0$.

Fragment Motion

In the present analysis, the fragment is assumed to be undeformable; hence, its equations of motion are

$$m_f\ddot{Y}_f = 0 \tag{13}$$

$$m_f\ddot{Z}_f = 0 \tag{14}$$

$$I_f\ddot{\psi} = 0 \tag{15}$$

where (Y_f, Z_f) and $(\ddot{Y}_f, \ddot{Z}_f)$ denote, respectively, the global coordinates and acceleration components of the center of gravity of fragment (see Fig. 4) and ψ represents the angular displacement of the fragment.

In timewise finite-difference forms, Eqs. (13–15) become

$$(\Delta\bar{Y}_f)_{j+1} = (\Delta Y_f)_j \tag{16}$$

$$(\Delta\bar{Z}_f)_{j+1} = (\Delta Z_f)_j \tag{17}$$

$$(\Delta\bar{\psi})_{j+1} = (\Delta\psi)_j \tag{18}$$

where the overbar signifies a trial value which requires modification, as explained later, if ring-fragment collision occurs between t_j and t_{j+1}.

Solution Procedure

The following procedure indicated in the flow diagram of Fig. 5 (and described also in Refs. 8 and 19) may be employed to predict the motion of the ring and the rigid fragment, their possible collision, the resulting collision-imparted velocities experienced by each, and the subsequent motion of each body.

Step 1

Let it be assumed at instant t_j that the coordinates $\{q^*\}_j$, $(Y_f)_j$, and $(Z_f)_j$, and coordinate increments $\{\Delta q^*\}_j$, $(\Delta Y_f)_j$, and $(\Delta Z_f)_j$ are known. One can then calculate the strain increments, $\Delta\epsilon_j$, at all Gaussian stations along and through the thickness of the ring, from the strain-displacement relations.

Step 2

Using a suitable constitutive relation for the ring material, the stress increments, $\Delta\sigma_j$, at corresponding depthwise and spanwise Gaussian stations can be determined from the now-known strain increments $\Delta\epsilon_j$ (see Ref. 8). Since the σ_{j-1} are known at time instant t_{j-1}, the stresses at t_j are given by $\sigma_j = \sigma_{j-1} + \Delta\sigma_j$. This information per-

§See Ref. 8 for criteria for selecting an appropriate Δt size.

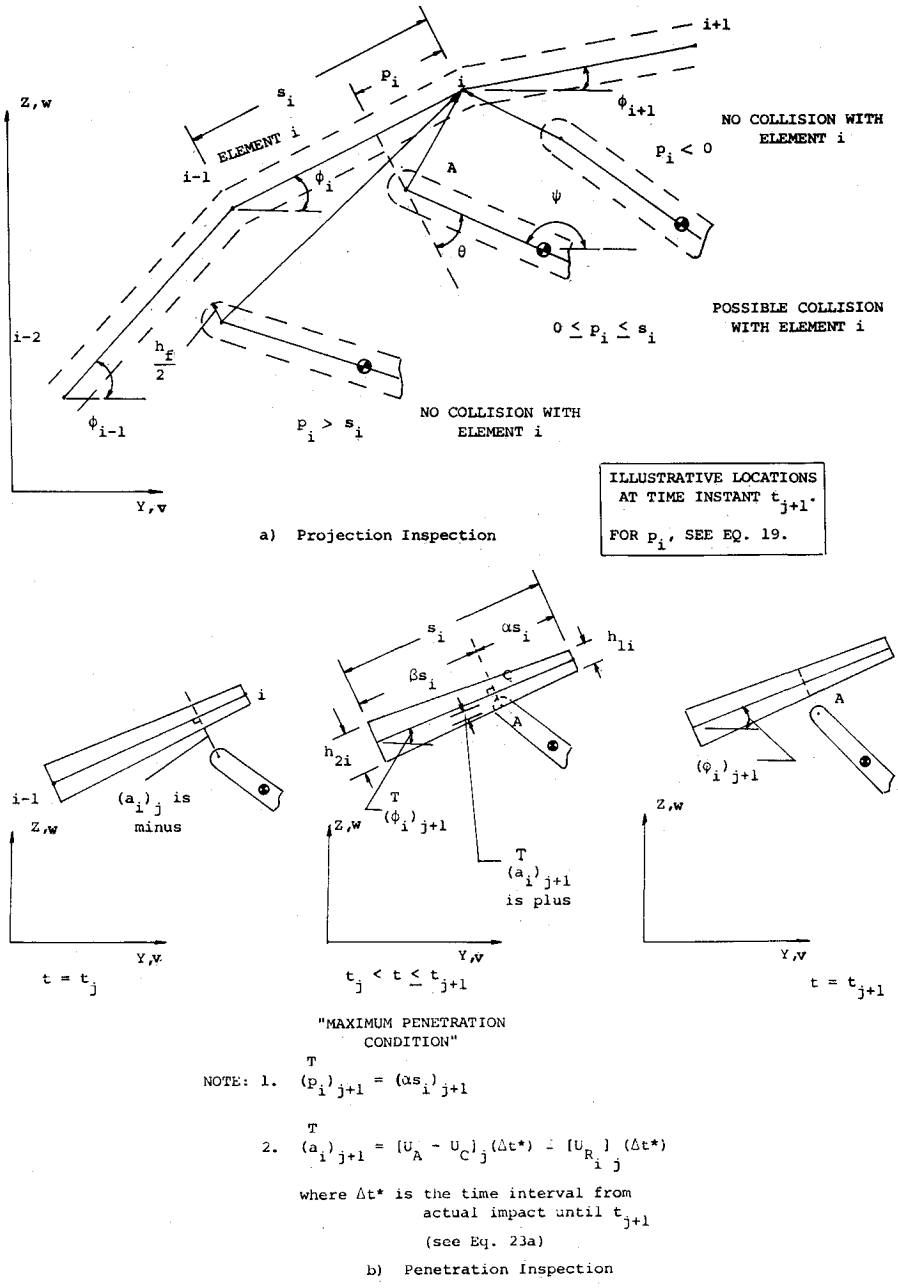

Fig. 4 Inspection for determining a collision of the fragment with the ring ("T" above letter in Fig. 4b equivalent to overbar in text).

mits determining the quantities $\{P^*\}$ and $[H^*]$ on the right-hand side of Eq. (12), where for the present problem $\{F^*\}_j$ is regarded as being zero.

Step 3

Solve Eq. (12) for the trial ring displacement increments $\{\Delta\bar{q}^*\}_{j+1}$. Also, use Eqs. (16–18) for the trial fragment displacement increments $(\Delta\bar{Y}_f)_{j+1}$, $(\Delta\bar{Z}_f)_{j+1}$, and $(\Delta\bar{\psi})_{j+1}$.

Step 4

Since a ring-fragment collision may have occurred between t_j and t_{j+1}, the following sequence of substeps may be employed to determine whether or not a collision occurred and, if so, to effect a correction of the coordinate increments of the affected ring segment and of the fragment.

Step 4a:

To check the possibility of a collision between the fragment in the vicinity of point A of the fragment with ring element i (approximated as a straight beam) as depicted in Fig. 4, compute the trial projection $(\bar{p}_i)_{j+1}$ of the line from ring node i to point A of the fragment, upon the straight line connecting ring nodes i and $i-1$, as follows, at time instant t_{j+1}

$$(\bar{p}_i)_{j+1} = (\bar{Y}_i - \bar{Y}_A)_{j+1}\cos(\bar{\phi})_{j+1} + (\bar{Z}_i - \bar{Z}_A)_{j+1}\sin(\bar{\phi})_{j+1} \tag{19}$$

where the Y,Z are inertial Cartesian coordinates. Now, examine $(\bar{p}_i)_{j+1}$; three cases are illustrated in Fig. 4a.

Step 4b

If $(\bar{p}_i)_{j+1} < 0$ or if $(\bar{p}_i)_{j+1} > s_i$, a collision between the fragment near point A and ring element i is impossible. Proceed to check ring element $i+1$, etc. for the possibility of a collision of fragment end A with other ring elements.

Step 4c

If $0 \leq (\bar{p}_i)_{j+1} \leq s_i$, a collision with ring element i is possible, and further checking is pursued. Next, calculate the fictitious penetration distance $(\bar{a}_i)_{j+1}$ of the fragment at end A into ring element i by (see Fig. 4b)

$$(\bar{a}_i)_{j+1} = 1/2[h_{1i} + \alpha(h_{2i} - h_{1i}) + h_f]_{j+1} - (\bar{d}_i)_{j+1} \quad (20)$$

where $\frac{1}{2}[h_{1i} + \alpha(h_{2i} - h_{1i})]$ = local semi-thickness of the ring element which is approximated as a straight beam in this collision calculation, $h_f/2$ = tip radius of the fragment at the impact end A, $\alpha_{j+1} = (\bar{p}_i/s_i)_{j+1}$ = fractional distance of s_i from node i to where the collision occurs (recall: $\alpha + \beta = 1$)

$$(\bar{d}_i)_{j+1} = -[\bar{Y}_i - \bar{Y}_A]_{j+1} \sin(\bar{\phi}_i)_{j+1} + [\bar{Z}_i - \bar{Z}_A]_{j+1} \cos(\bar{\phi}_i)_{j+1} \quad (21)$$

= the projection of the line connecting node i with point A upon a line perpendicular to the line joining nodes i and $i-1$.

Next, examine $(\bar{a}_i)_{j+1}$ which is indicated schematically in Fig. 4b and is given by Eq. (20).

Step 4d

If $(\bar{a}_i)_{j+1} \leq 0$, no collision of the fragment near point A upon element i has occurred during the time interval from t_j to t_{j+1}. Hence, one can proceed to check element $i + 1$, etc. for the possibility of a collision of fragment end A with other ring elements.

Step 4e

If $(\bar{a}_i)_{j+1} > 0$, a collision has occurred; corrected coordinate increments (boldface letters) may be determined approximately by (see Fig. 4b)

$$(\Delta v_f)_{j+1} = (\Delta \bar{v}_f)_{j+1} + (\Delta t^*)[U_f' - U_f] \sin(\bar{\phi}_i)_{j+1} \quad (22a)$$

$$(\Delta w_f)_{j+1} = (\Delta \bar{w}_f)_{j+1} - (\Delta t^*)[U_f' - U_f] \cos(\bar{\phi}_i)_{j+1} \quad (22b)$$

$$(\Delta \psi)_{j+1} = (\Delta \bar{\psi})_{j+1} + (\Delta t^*)[\omega_f' - \omega_f] \quad (22c)$$

$$(\Delta v_{i-1})_{j+1} = (\Delta \bar{v}_{i-1})_{j+1} - (\Delta t^*)[U_2' - U_2] \sin(\bar{\phi}_i)_{j+1} \quad (22d)$$

$$(\Delta w_{i-1})_{j+1} = (\Delta \bar{w}_{i-1})_{j+1} + (\Delta t^*)[U_2' - U_2] \cos(\bar{\phi}_i)_{j+1} \quad (22e)$$

$$(\Delta v_i)_{j+1} = (\Delta \bar{v}_i)_{j+1} - (\Delta t^*)[U_1' - U_1] \sin(\bar{\phi}_i)_{j+1} \quad (22f)$$

$$(\Delta w_i)_{j+1} = (\Delta \bar{w}_i)_{j+1} + (\Delta t^*)[U_1' - U_1] \cos(\bar{\phi}_i)_{j+1} \quad (22g)$$

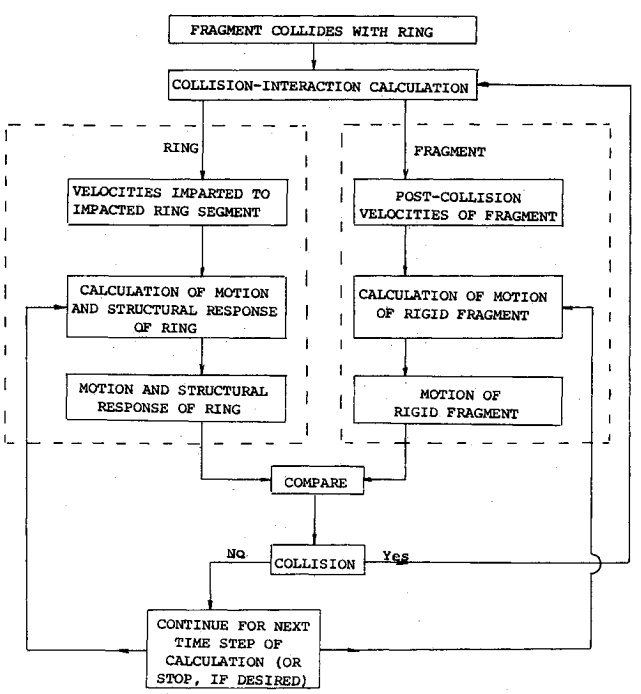

Fig. 5 Information flow schematic for predicting ring and fragment motions in the CIVM approach.

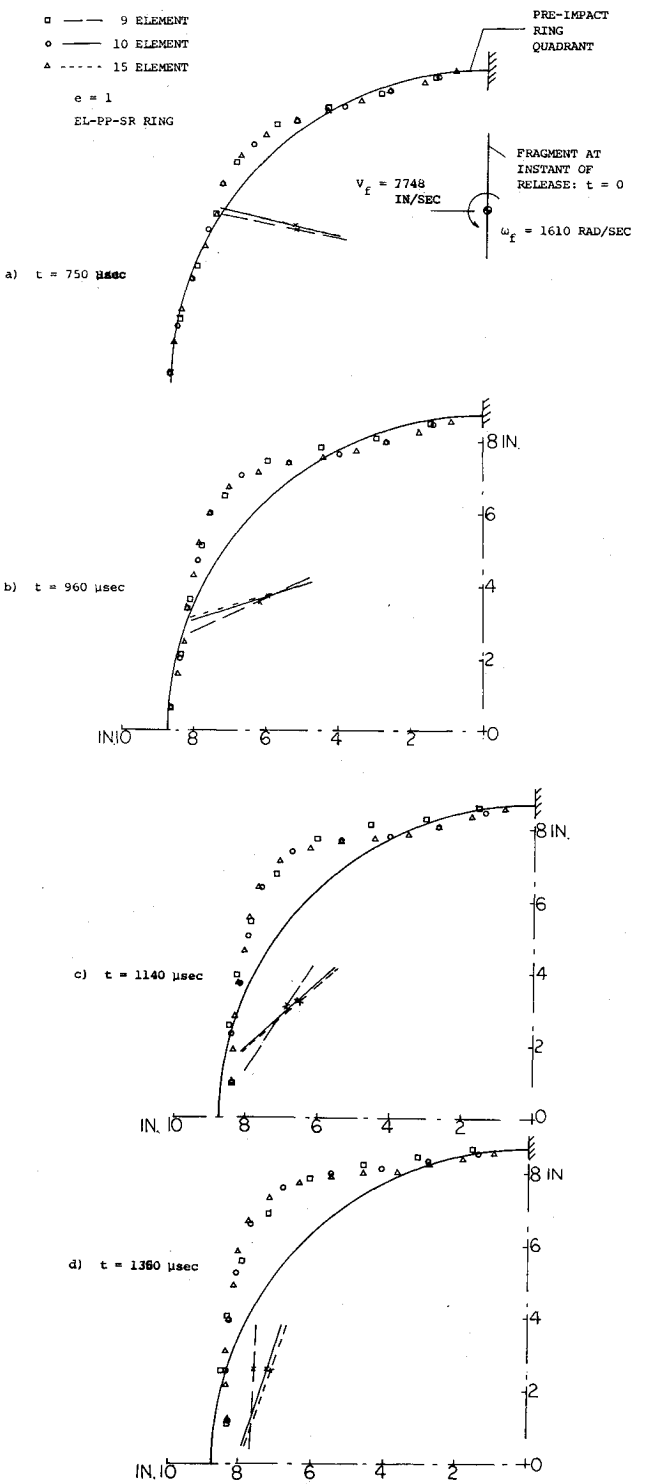

Fig. 6 Ring quadrant and blade fragment responses predicted by using the present collision model.

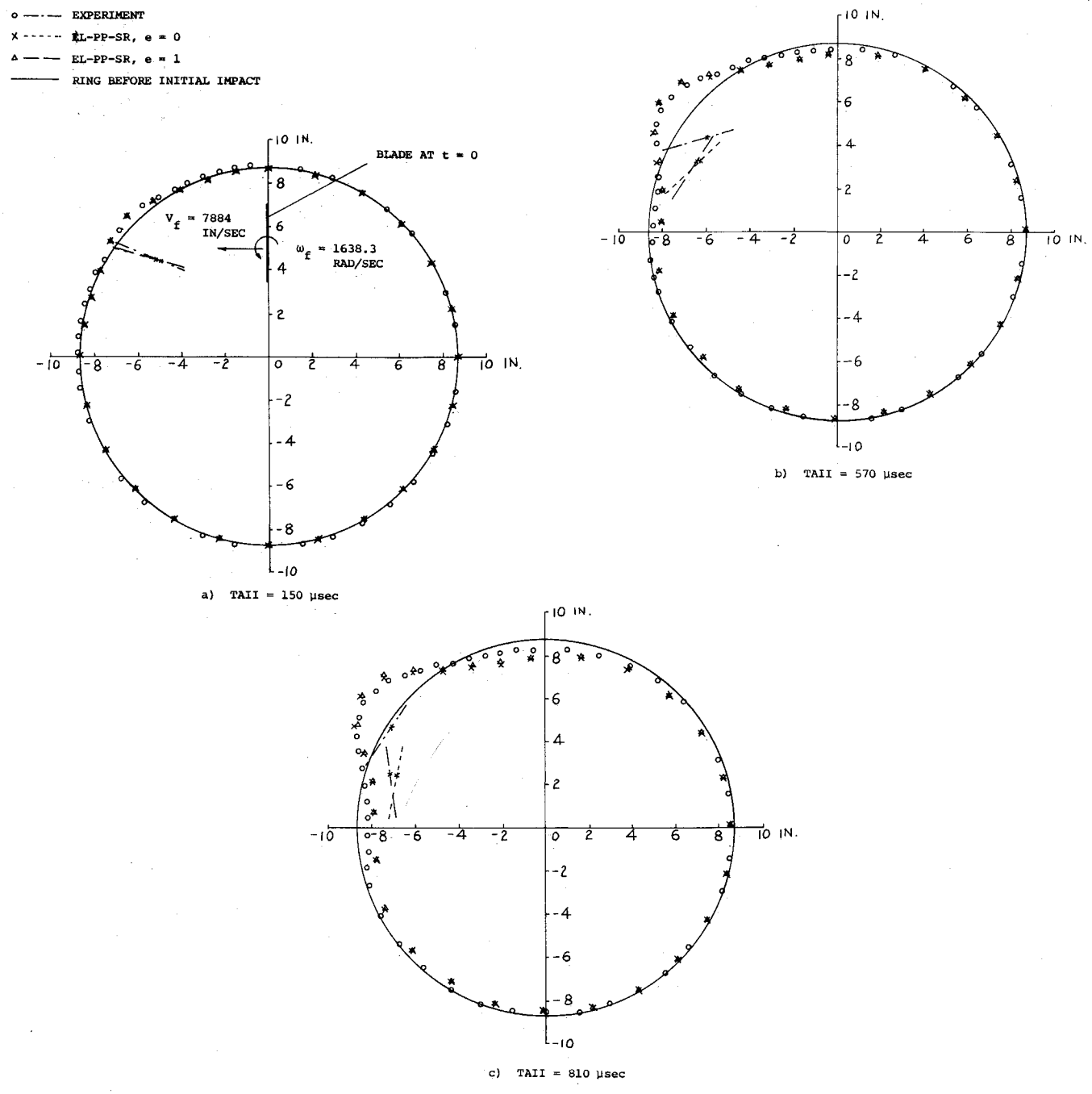

Fig. 7 Comparison of predictions with experimental for the free complete ring subjected to single-blade impact in NAPTC Test 91.

where the after-impact quantities U_1', U_2', U_f', and ω_f' may be found, respectively, from Eqs. (7–10), and where

$$\Delta t^* = (\bar{a}_i)_{j+1}/(U_{Ri})_j = \text{time interval from actual impact on ring element } i \text{ until } t_{j+1} \tag{23a}$$

$$(U_{Ri})_j = -[\beta_{j+1}(U_1)_j + \alpha_{j+1}(U_2)_j] + [(U_f)_j - (\omega_f)_j l \sin\theta] = \text{preimpact relative velocity of points } A \text{ and } C \tag{23b}$$

The terms, in Eqs. (22a–22g), which are multiplied by (Δt^*) represent corrections to the trial incremental quantities for the (Δt^*) time interval. Also, since Δt is small, one may use either angle $(\bar{\phi}_i)_{j+1}$ or angle $(\phi_i)_j$ in Eqs. (22a–22g).

Step 5

Having determined the corrected coordinate increments¶ for the impacted ring element, this time cycle of calculation is now complete. One then proceeds to calculate the ring nodal coordinate increments and the fragment coordinates for the time step from t_{j+1} to t_{j+2}, starting with Step 1. The process proceeds cyclically thereafter for as many time increments as desired.

If, however, one finds no collision of fragment end A

¶It should be noted that in this approximate calculation, only the coordinate increments of the fragment and of the impacted ring segment are corrected. Those for all other ring segments are regarded as already being correct. The time increment Δt is regarded as being sufficiently small to make these approximations acceptable.

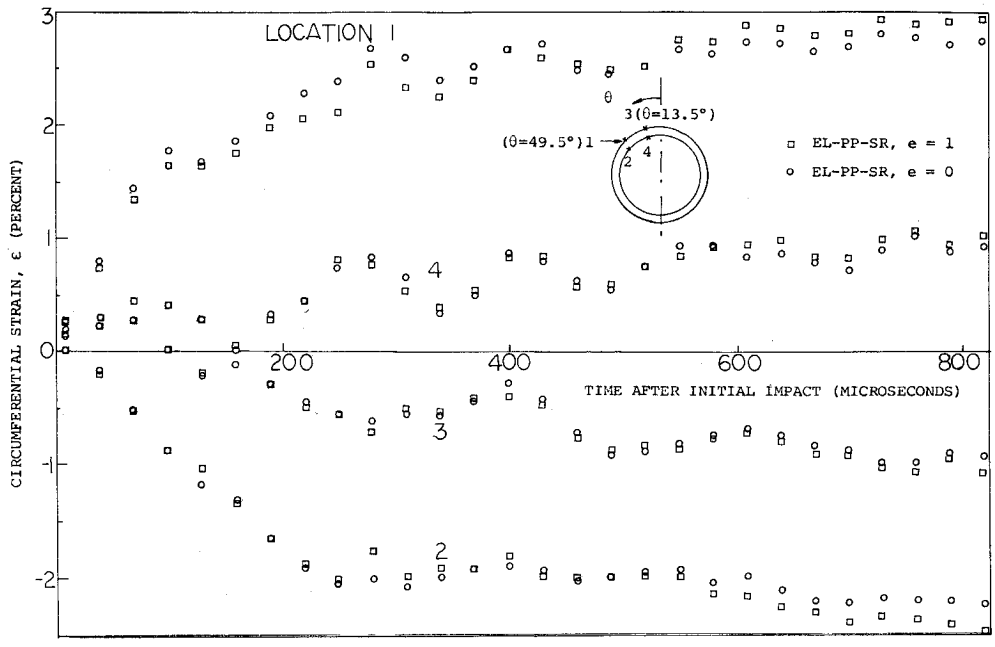

Fig. 8 Effect of the coefficient of resitution on the predicted inner-surface and outer-surface circumferential strains of a blade-impacted free complete ring.

with any of the ring segments, the checking process should be repeated for any other possible fragment points of impact (such as end B, for example) with the ring.

This solution procedure may be carried out for as many time steps as desired or may be terminated by invoking the use of a termination criterion such as, for example, the reaching of a critical value of the strain at the inner surface or the outer surface of the ring. Appropriate modifications of this approximate analysis could be made, if desired, to follow the behavior of the ring and the fragment after the initiation and/or completion of local facturing of the ring has occurred.

Evaluation and Discussion

To illustrate the present first-cut analysis procedure, example problems have been analyzed, which involve the impact of a single rotor blade (fragment) against a) a free complete circular containment ring and b) a fragment-deflection ring quadrant which is supported at a selected station in one of several ways. For the complete-ring example, preliminary experimental ring response data (Ring Tests No. 88 and 91 from the Naval Air Propulsion Test Center[6,10,11]) are available for comparison with predictions. However, no experimental data are available for the ring quadrant cases.

The free containment ring consisted of 2024-T4 aluminum with dimensions 17.619-in outside diam, 0.152-in radial thickness, and 1.506-in axial length; its uniaxial static stress-strain behavior was approximated as being elastic, perfectly-plastic (EL-PP) with a yield stress, σ_0, of 50,000 psi and elastic modulus of 10^7 psi. Also, it is assumed that strain rate (SR), $\dot{\epsilon}$, raises the static yield stress, approximately as follows

$$\sigma_y = \sigma_0\left(1 + \left|\frac{\dot{\epsilon}}{D}\right|^{1/p}\right) \tag{24}$$

where σ_y is the strain-rate-dependent uniaxial yield stress, D and p are constants which depend on the material involved. For aluminum, D = 6500 sec^{-1} and p = 4 are commonly used.

A single T-58 engine turbine rotor blade which was fabricated from material designated as SEL-15 by General Electric was the fragment employed and had the following characteristics: 0.084 lb weight, 3.5 in length, 1.657 in tip clearance,** 2.188 in length from its c.g. to tip, and 2.163×10^{-4} in-lb-sec^2 moment of inertia about its c.g. This fragment is treated as being rigid in the present analysis.

For the ring-quadrant example calculations, the same geometry and material properties were employed as for the complete-ring example.

First, consider the ring quadrant clamped at one end; 9, 10, and 15 equal-length elements were used to model the ring quadrant and e = 1(perfectly-elastic impact) was employed for the coefficient of restitution. The predicted responses[8] of the ring quadrant and of the blade at a sequence of times are illustrated in Fig. 6; the preimpact c.g. translational and the rotational velocity used for the fragment are also shown in Fig. 6. The plotted points represent the locations of the node points of the finite elements into which the ring quadrant has been discretized for analysis. Note that the 9-element result differs somewhat from the 10-element result, but the 10-element and the 15-element results are nearly the same; this suggests that the 10-element calculation gives a converged solution.†† These results provide a tentative guidance for selecting a sufficiently fine space mesh. Also this example illustrates only a few of the many possible situations and configurations which may be worthy of study for fragment-deflection purposes.

Similar predicted ring profiles and blade locations[8] at a sequence of times after initial impact (TAII) for single-blade impact upon a free complete ring are illustrated in Fig. 7 for both perfectly-elastic impact (e = 1) and perfectly-inelastic impact (e = 0); the preimpact cg translational and the rotational velocity of the fragment are shown in Fig. 7. The free (complete) ring was discretized by 28 elements: 10 elements in the quadrant where impact occurs and 6 elements in the other three quadrants; this discretization is assumed to provide a converged result.‡‡ The strain responses predicted on both the outer surface and the inner surface of the ring at two interesting

**This tip clearance is much larger than normal, but is used here to illustrate the method and to compare with available experimental data.

††Space limitations preclude further discussion of the convergence question (see Ref. 8).

‡‡Further details of the finite elements and modeling are given in Ref. 8. For this finite element modeling of the ring (112 degrees of freedom) and Δt = 1.0 μsec, the computing time on the IBM 370/155 at MIT for 820 μsec of structural response was 4.7 min.

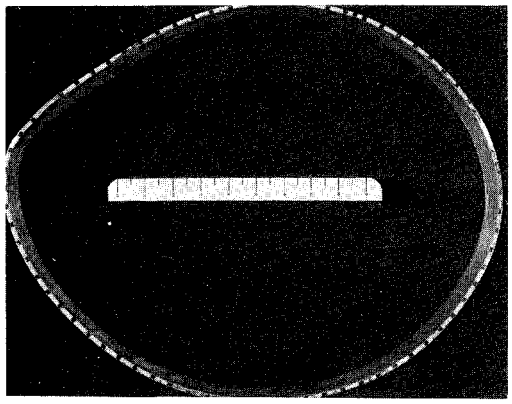

a) Deformed containment ring

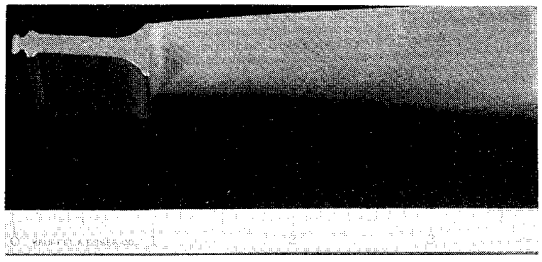

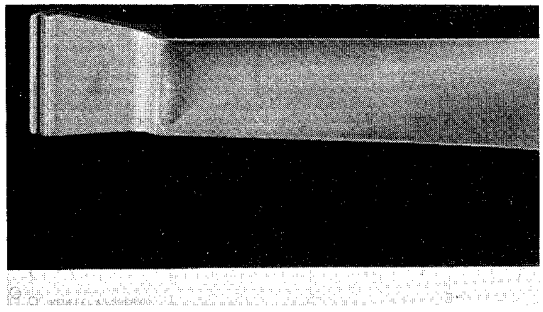

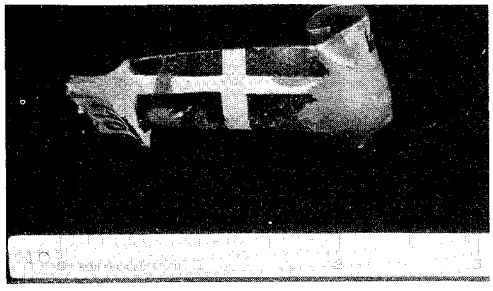

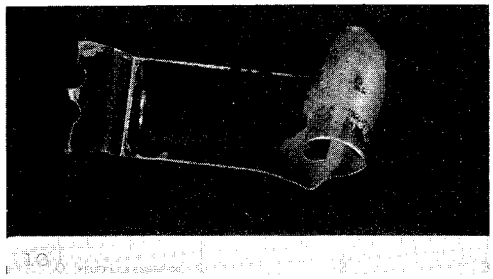

b) Blade fragments

Fig. 9 Illustration of blade fragments and a deformed containment ring.

θ-locations (θ = 13.5° and 49.5°) are shown in Fig. 8. It should be noted that initial impact occurs at θ = 44.5°; in regions well removed from the impact zone, the predicted strains are very small. However, no measured strain histories are available for comparison. On the other hand, it is seen from Fig. 7 that the predicted ring deformation responses agree fairly well with experimental measurements from NAPTC Test 91, but the predicted blade motion is not in satisfactory agreement with experimental observations.

Finally, to illustrate more concretely the type of blade fragment under discussion, and containment ring deformation, Fig. 9 shows an undeformed blade as well as the post-test deformed blade and deformed ring[6] for NAPTC Test 146 which was quite similar to the conditions of NAPTC Test 91 the data from which have been used in the present comparisons.

Concluding Comments

As for the ring itself, the method of large deflection elastic-plastic transient response analysis has been evaluated and its accuracy verified by comparison with reliable experimental data in Refs. 7 and 8 and, hence, is not a source of significant error. However, one source of error is readily apparent: in the experiments, the rotor blade fragment undergoes a significant amount of deformation over the portion of its length near the impact tip during a brief period following initial impact; little further blade deformation is observed at later times—this factor probably accounts for much of the discrepancy between the observed and the predicted blade motion. Other neglected factors include the roughness of the ring-fragment impact surfaces, and tangential forces arising from and energy loss associated with rubbing or gouging of the ring by the blade. These deficiencies in the simplifying assumptions contained in the present analysis (which were invoked to expedite the present study) could all be removed in future work and would likely lead to improved qualitative and quantitative predictions. Some of these matters (tangential forces and friction, for example) are explored in Ref. 18 which pertains to the CFM-type of analysis.

Also worthy of future investigation are the effects of more complicated fragments upon containment structures or upon various types of fragment deflection devices. Fragments of practical interest include 1) a single blade from a fully-bladed rotor and 2) a fragment consisting of a portion of the turbine disk's rim with perhaps 3–10 blades attached. Finally, the inclusion of the actual nonplanar deformation behavior of a containment vessel, which will occur if its axial length is significantly greater than the fragment's axial-projection length, should be treated in both analysis and experiments since this factor may have an important bearing upon determining a least-weight containment structure.

References

[1]Chiarito, P. T., "Status of Engine Rotor Burst Protection Program for Aircraft," *NASA Aircraft Safety and Operating Problems Conference*, NASA SP-270, May 4–6, 1971.

[2]Martino, A. A. and Mangano, G. J., "Turbine Disk Burst Protection Study. Phase I—Final Report on Problem Assignment NASA DPR R-105," NAEC-AEL-1793, NASA CR-80962, March 1965, U.S. Navy.

[3]Martino, A. A. and Mangano, G. J., "Turbine Disk Burst Protection Study. Phases II and III—Final Report on Problem Assignment NASA DPR R-105," NAEC-AEL-1848, NASA CR-84967, Feb. 1967, U.S. Navy.

[4]Martino, A. A. and Mangano, G. J., "Rotor Burst Protection Program Initial Test Results. Phase IV—Final Report [on Problem Assignment] NASA DPR R-105," NAPTC-AED-1869, NASA CR-95967, April 1968, U. S. Navy.

[5]Martino, A. A. and Mangano, G. J., "Rotor Burst Protection

Program. Phase V—Final Report [on] Problem Assignment NASA DPR R-105," NAPTC-AED-1901, NASA CR-106801, May 1969.

[6]Martino, A. A. and Mangano, G. J., private communication, 1970–1972, Naval Air Propulsion Test Center, Philadelphia, Pa.

[7]Balmer, H. A. and Witmer, E. A., "Theoretical-Experimental Correlation of Large Dynamic and Permanent Deformations of Impulsively-Loaded Simple Structures," AFFDL-TDR-64-108, July 1964, MIT, Cambridge, Mass.

[8]Wu, R. W-H. and Witmer, E. A., "Finite-Element Analysis of Large Transient Elastic-Plastic Deformations of Simple Structures, with Application to the Engine Rotor Fragment Containment/Deflection Problem," ASRL TR 154-4, NASA CR-120886, Jan. 1972, Aeroelastic and Structures Research Lab., MIT, Cambridge, Mass.

[9]Wu, R. W-H. and Witmer, E. A., "Finite-Element Analysis of Large Elastic-Plastic Transient Deformations of Simple Structures," *AIAA Journal*, Vol. 9, No. 9, Sept 1971, pp. 1719–1724.

[10]McCallum, R. B., Leech, J. W. and Witmer, E. A., "Progress in the Analysis of Jet Engine Burst-Rotor Containment Devices," ASRL TR 154-1, NASA CR-107900, Aug. 1969, Aeroelastic and Structures Research Lab., MIT, Cambridge, Mass.

[11]McCallum, R. B., Leech, J. W. and Witmer, E. A., "On the Interaction Forces and Responses of Structural Rings Subjected to Fragment Impact," ASRL TR 154-2, NASA CR-72801, Sept. 1970, Aeroelastic and Structures Research Lab., MIT.

[12]Simon, J. A. and Moriarty, D., Private Communication, April 1971, General Electric Co., Evendale Div., Cincinatti, Ohio.

[13]Leech, J. W., Witmer, E. A. and Yeghiayan, R. P., "Dimensional Analysis Considerations in the Engine Rotor Fragment Containment/Deflection Problem," ASRL TR 154-3, NASA CR-120841, Dec., 1971, Aeroelastic and Structures Research Lab., MIT, Cambridge, Mass.

[14]Yeghiayan, R. P., Witmer, E. A., and Leech, J. W., "Theoretical and Experimental Studies of the Interaction Forces and Responses of Structural Rings Subjected to Engine Rotor Fragment Impact," ASRL TR 154-5, (in preparation), Aeroelastic and Structures Research Lab., MIT, Cambridge, Mass.

[15]Wilkins, M. L., "Calculation of Elastic-Plastic Flow," UCRL-7322, Rev. I, Jan. 1969, Lawrence Radiation Lab., Livermore, Calif. more, Calif.

[16]Kreyenhagen, K. N., Read, H. E., Rosenblatt, M. and Moore, W. C., "Hardening Technology Studies—III, STRIDE Code Solutions and Extension to Multi-material Systems," SAMSO-TR-69-16, Dec. 1968.

[17]Hageman, L. J and Walsh, J. M., "HELP: A Multimaterial Eulerian Program for Compressible Fluid and Elastic-Plastic Flows in Two Space Dimensions and Time," *Vol. I—Formulation and Vol. II—Fortran Listing of HELP*, BRL CR No. 39, May 1971, Systems, Science, and Software, La Jolla, Calif.

[18]Zirin, R. and Witmer, E. A., "Examination of the Collision Force Method for Analyzing the Responses of Simple Containment/Deflection Structures to Impact by One Engine Rotor Blade Fragment," ASRL TR 154-6, NASA CR-120952, May 1972, Aeroelastic and Structures Research Lab.. MIT, Cambridge, Mass.

[19]Balmer, H. A. and Witmer, E. A., "Theoretical-Experimental Correlation of Large Dynamic and Permanent Deformations of Impulsively-Loaded Unbonded Concentric Rings," AFFDL-TR-65-143, Nov. 1965, Aeroelastic and Structures Research Lab., MIT, Cambridge, Mass.

[20]Hibbitt, H. D., Marcal, P. V. and Rice, J. R., "A Finite Element Formulation for Problems of Large Strain and Large Displacement," Rept. N000/4-0007/2, June 1969, Div. of Engineering, Brown Univ., Providence, R.I.

[21]Stricklin, J. A., Martinez, J. E., Tillerson, J. R., Hong, J. H. and Haisler, W. E., "Nonlinear Dynamic Analysis of Shells of Revolution by the Matrix Displacement Method," Rept. 69–77, Feb. 1970, Dept. of Aerospace Engineering, Texas A & M Univ., College Station, Texas.